International Journal of Pharmaceutics: X 9 (2025) 100330

Contents lists available at ScienceDirect

International Journal of Pharmaceutics: X

journal homepage: www.sciencedirect.com/journal/international-journal-of-pharmaceutics-x

Enrofloxacin-silver composite nano-emulsion as a scalable synergetic antibacterial platform for accelerating infected wound healing

Jiahao Gong [a], Moxin Liu [b], Runan Zuo [c], Xinhao Song [d], Junqi Wang [a], Qindan Zuo [a], Yan Jiang [e], Yunfeng Long [e], Yuzhen Silang [f], Zeng Luo [f], Xiuge Gao [a], Dawei Guo [a,*]

[a] Engineering Center of Innovative Veterinary Drugs, Center for Veterinary Drug Research and Evaluation, MOE Joint International Research Laboratory of Animal Health and Food Safety, College of Veterinary Medicine, Nanjing Agricultural University, 1 Weigang, Nanjing 210095, China
[b] Shanghai Customs District, 13 Zhongshan East Road, Shanghai 200002, China
[c] Animal-Derived Food Safety Innovation Team, Anhui Province Key Lab of Veterinary Pathobiology and Disease Control, College of Animal Science and Technology, Anhui Agricultural University, Hefei 230036, China
[d] School of Traditional Chinese Pharmacy, China Pharmaceutical University, Nanjing 211100, China
[e] Animal, Plant and Food Inspection Center of Nanjing Customs District, 39 Chuangzhi Road, Nanjing 210000, China
[f] Institute of Grassland Science, Tibet Academy of Agriculture and Animal Husbandry Sciences, 130 Jinzhu West Road, Lhasa 850000, China

ARTICLE INFO

Keywords:
Bacterial infection
Enrofloxacin
Nanostructured lipid carriers
Silver nanoparticles
Antibacterial
Synergistic therapy
Wound healing

ABSTRACT

The colonization of bacterial pathogens is a major concern in wound infection and becoming a notable medical issue. Enrofloxacin (ENR) can be applied to treat skin infections, while poor water solubility and bioavailability limit its clinical application. Nanostructured lipid carriers (NLCs) enhance the solubility and bioavailability of drugs by encapsulating them, making them effective for the topical treatment of skin wound infections. Additionally, to enhance treatment efficacy and further improve wound healing, silver nanoparticles (AgNPs) were attached to the aforementioned matrix, which also improved its colloidal stability and reduced toxicity. Herein, a scalable poly (vinyl alcohol) modified NLCs-based antibacterial platform was fabricated by high-pressure homogenization method, to co-load ENR and AgNPs for treating the bacterial-infected wounds. The growth of common wound bacterial pathogens (*Escherichia coli*, *Staphylococcus aureus* and *Pseudomonas aeruginosa*) was synergistically inhibited by released ENR and Ag^{+} from the poly (vinyl alcohol) modified enrofloxacin-silver composite nano-emulsion (ENR@PVA-NLCs/AgNPs). In the *in vivo* wound model, the *Staphylococcus aureus*-infected wound in rat almost completely disappeared after treatment with ENR@PVA-NLCs/AgNPs, and no suppuration symptom was observed. Importantly, this nanoplatform had negligible side effects *in vivo*. Taken together, the above results strongly demonstrate the promising potential of ENR@PVA-NLCs/AgNPs as a synergistic therapeutic agent for clinical wound infections.

1. Introduction

The skin is an essential part of the innate immune system, and protects the human and animal body from external damage (Suo et al., 2021). However, the skin is easily damaged by mechanical forces, leading to a loss of skin integrity and generating wounds. It's worth noting that wounds are susceptible to bacterial pathogens, resulting in delayed healing, chronic wounds, septicemia, or even systemic inflammatory response syndrome, which has become a notable medical threat and caused immense financial burden to healthcare systems worldwide (Yang et al., 2021; Zheng et al., 2022).

Traditionally, antibiotics have been the mainstay in treating wound infections (Dubourg et al., 2017). Enrofloxacin (ENR), a fluoroquinolone antibiotic, has broad-spectrum antibacterial activity and is widely applied to treat bacterial infection in livestock, poultry and pet (Ruennarong et al., 2016). However, the poor solubility and rapid metabolism limit its clinical application. The need for repeated high doses in clinical settings can lead to significant side effects and contribute to drug resistance. To improve its solubility and sustained release and realize doses decreasing and efficacy increasing, scientists have developed many innovative enrofloxacin-based nano formulations in recent years (Liang and Chen, 2022; Liu et al., 2021; Meng et al., 2020). For instance, Paudel et al. synthesized polymer-based nanoparticles of poly (lactide-*co*-glycolide) (PLGA) and lignin-*graft*-PLGA

* Corresponding author.
E-mail address: gdawei0123@njau.edu.cn (D. Guo).

https://doi.org/10.1016/j.ijpx.2025.100330
Received 13 December 2024; Received in revised form 5 March 2025; Accepted 22 March 2025
Available online 25 March 2025

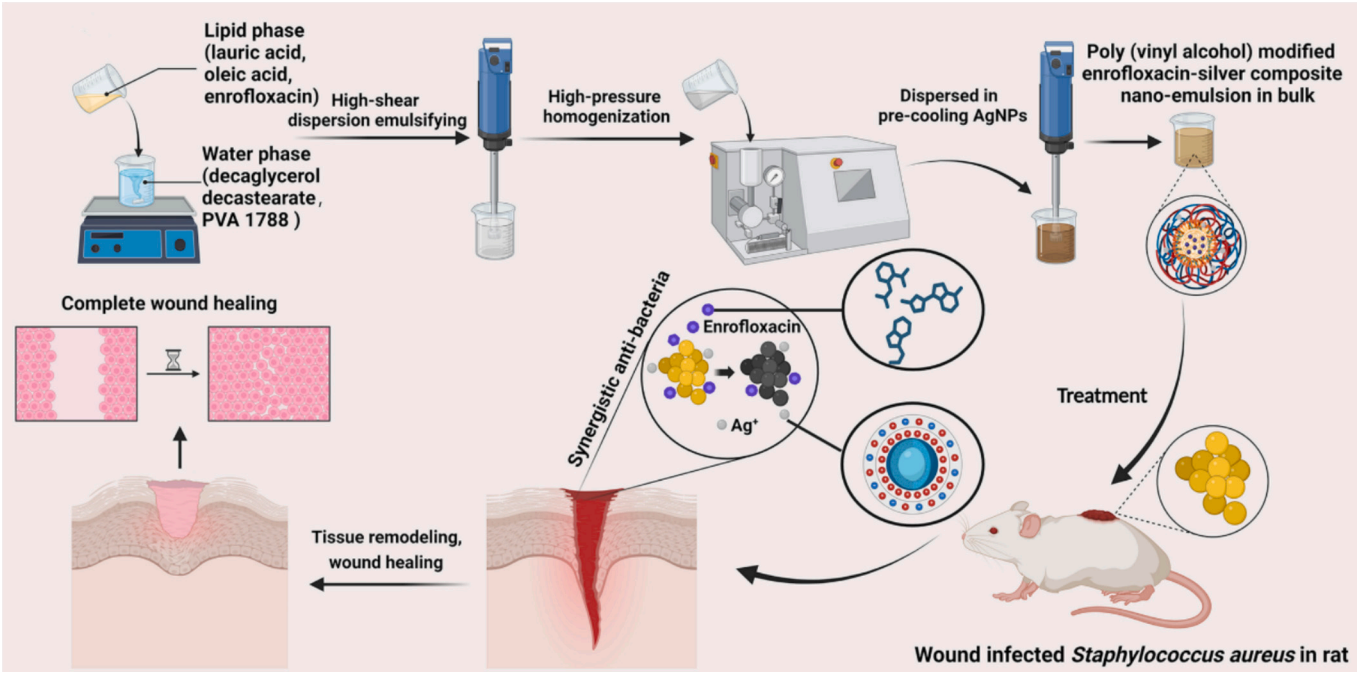

Scheme 1. Schematic illustration of the antibacterial nanoplatform of enrofloxacin-silver composite nano-emulsion (ENR@PVA-NLCs/AgNPs) for synergistically promoting wound healing.

loaded with ENR, and found the nanoparticles presented better bacterial infection treatment and prevention efficacy (Paudel et al., 2021). Tao et al. developed an ENR-loaded solid lipid nanoparticle suspension as oral and intramuscular sustained release formulations for pig and enhance the bioavailability of ENR (Tao et al., 2019). However, studies on topical formulations of ENR for infected wound healing are relatively scarce (Liang and Chen, 2022; Luo et al., 2023), and complex preparation processes and high costs limit their clinical potential. Hence, the development of a novel topical formulation of ENR with a simple and cost-effective synthesis process is urgent to treat wound bacterial infection.

Nanostructured lipid carriers (NLCs) are widely used to encapsulate drugs to improve solubility and bioavailability (Gao et al., 2021). These carriers are also suitable delivery systems for the topical treatment of skin diseases (Gainza et al., 2014). Moreover, their small particle size and lipidic composition ensure close contact between the nanoparticles and the skin, the release of the encapsulated drugs in a controlled manner, and an increase in their residence time in the skin (Gokce et al., 2012). What's more, our previous report showed that NLCs could be scaled up by high-pressure homogenization technique (Xu et al., 2024), together with the lack of organic solvents, and lower production cost, which enable the possibility of commercialization (Khairnar et al., 2022). Above characteristics make the use of NLCs as drug delivery systems an available strategy for treating infected wounds.

It is well-known that nanoparticle's surface chemical properties can also influence its therapeutic efficacy, except for particle size and morphology (Du et al., 2018). The surface modification of nanoparticle can enhance the stability of delivery carrier and the bioavailability of encapsulated drug (Bochicchio et al., 2021). Poly (vinyl alcohol) (PVA), a water-soluble polymer that has widely been used as a component of biomaterials, including wound dressings (Khutoryanskiy, 2018), based on its mechanical properties, emulsifying, good compatibility and biodegradability in human and animal tissues and fluids (Rolim et al., 2019).

In addressing the complexities of wound environments, designing antibacterial dressings demands a targeted approach for synergistic treatments (Ibraheem et al., 2024; Ibraheem et al., 2022; Jawad et al., 2024; Li et al., 2022). Silver is famous for its potent antibacterial properties, and it has been used in different forms like metallic silver, silver nitrate, silver sulfadiazine for treating bacterial infections in wounds (Rai et al., 2009). Among them, silver nanoparticles (AgNPs) have better scarless wound healing capacity (Jiji et al., 2020). AgNPs were also recently demonstrated to have the feature of enhanced epidermal re-epithelialization (Liu et al., 2010). In particular, AgNPs were found to improve inflammatory cell infiltration, fibroblast proliferation and new collagen synthesis on injured animal tissues (Pallavicini et al., 2017). However, fast ions release, narrow safety range, and poor stability limit their applications (Lee and Jun, 2019). Attaching or embedding AgNPs into organic/inorganic matrix is an excellent strategy to endow them with enhanced colloidal stability and reduced toxicity (He et al., 2022; Pang et al., 2024).

In this work, poly (vinyl alcohol) modified NLCs loaded ENR and AgNPs ((poly (vinyl alcohol) modified enrofloxacin-silver composite nano-emulsion, ENR@PVA-NLCs/AgNPs) was prepared by high pressure homogenization for synergistically inhibiting bacterial proliferation and promoting wound healing (Scheme 1). *In vitro*, the released ENR and Ag^{+} from ENR@PVA-NLCs/AgNPs could enhance the bactericidal effect. *In vivo*, ENR@PVA-NLCs/AgNPs showed excellent bacteria killing activity, promoting wound healing, and good biocompatibility in an *S. aureus*-infected wound model. Therefore, the antibacterial nanoplatform, ENR@PVA-NLCs/AgNPs, might be a promising wound dressing for skin infection treatment.

2. Experimental sections

2.1. Materials

Ganoderma extract (Ge, *Ganoderma* lucidum polysaccharide, 80 %) and silver nitrate were purchased from Ci Yuan Biotechnology Co., Ltd. (Xi'an, China) and Sinopharm Chemical Reagent Co., Ltd. (Shanghai, China), respectively. Glycerol monolaurate (GML), oleic acid (OA), decaglycerol decastearate, poly (vinyl alcohol) 1788 were obtained from Aladdin Biochemical Technology Co., Ltd. (Shanghai, China). Enrofloxacin (ENR, MW: 359.40) was provided by Huijiecheng

Biotechnology Co., Ltd. (Nanjing, China). Müller-Hinton (MH) and Luria-Bertani (LB) medium were purchased from Haibo Biological Co., Ltd. (Qingdao, China). *Escherichia coli* (*E. coli* ATCC 25922), *Staphylococcus aureus* (*S. aureus* ATCC 29213) and *Pseudomonas aeruginosa* (*P. aeruginosa* ATCC 9027) were preserved in our laboratory. Cells from the BJ human skin fibroblast cell line was obtained from the Chinese Academy of Sciences Typical Culture Preservation Committee cell bank and cultured in Dulbecco's modified Eagle's medium (DMEM) with 10 % fetal bovine serum (FBS) at 37 °C with 5 % CO_2.

2.2. Synthesis of silver nanoparticles

The silver nanoparticles (AgNPs) were synthesized by a biological method, referring to the previous study we reported with some modification (Gong et al., 2023). In this work, a *Ganoderma* extract (*Ganoderma* lucidum polysaccharide, 80 %) was prepared using hot water extraction method, which served as both a reducing and capping agent for the synthesis of AgNPs. In a three-necked round-bottomed flask, 3 g/L of Ge solution was heated up to 90 °C under magnetic stirring, and then an equal volume of $AgNO_3$ solution (4 mM) was rapidly poured in for 4 h.

2.3. Preparation of poly (vinyl alcohol) modified enrofloxacin-silver composite nano-emulsion (ENR@PVA-NLCs/AgNPs)

The ENR@PVA-NLCs/AgNPs were prepared according to high-pressure homogenization methods. As shown in Scheme 1A, 0.25 g of ENR, 0.6 g of GML, and 0.4 g of OA were mixed at 500 rpm, 80 °C to obtain the oil phase. The poly (vinyl alcohol) 1788 solution (1 %, w/v) containing decaglycerol decastearate was heated at 80 °C under magnetic stirring. Then, the oil phase was promptly transferred into the above-mentioned poly (vinyl alcohol) 1788 solution. Subsequently, the mixture was emulsified by a High Shear Dispersion Emulsifying Machine (FM200, IKA, Staufen, Germany) at 15000 rpm for 5 min. The obtained pre-emulsion was circulated five times in a High-Pressure Homogenizer (AH-BASIC, IS, Suzhou, China) at 700 bar, and the hot homogenized emulsion was dispersed into an equal volume of pre-cooling AgNPs under high-shear conditions for 1 min. Finally, the mixture was kept in an ice bath for 10 min to solidify the particles and obtain ENR@PVA-NLCs/AgNPs.

2.4. Characterization of ENR@PVA-NLCs/AgNPs

2.4.1. Transmission electron microscopy (TEM)

The morphology of AgNPs, ENR@PVA-NLCs and ENR@PVA-NLCs/AgNPs was observed by transmission electron microscopy (TEM; H-7650, Hitachi, Tokyo, Japan). Briefly, the diluted samples were dropped onto 200-mesh copper grids. After drying, the samples were negatively stained for 2 min using a 2 % (w/v) phosphotungstic acid solution. The dried samples were then subjected to TEM analysis.

2.4.2. Scanning electron microscopy (SEM)

The AgNPs, ENR@PVA-NLCs and ENR@PVA-NLCs/AgNPs aqueous solution was dropped on the silicon wafer, air-dried and then Pt was sputtered on its surface. Scanning electron microscopy (SEM; SU8600, Hitachi, Tokyo, Japan) were used to observe the morphology of nanoparticles.

2.4.3. Hydrodynamic diameter, polydispersity index, and zeta potential

The hydrodynamic diameter, polydispersity index and *zeta* potential of AgNPs, ENR@PVA-NLCs and ENR@PVA-NLCs/AgNPs were determined by a Zetasizer Nano ZSE (Malvern Instruments, Worcestershire, UK). The diluted samples were measured with scattering angles of 90° at 25 °C.

2.4.4. Fourier transform infrared spectroscopy (FT-IR)

Fourier transform infrared (FT-IR) spectra were recorded using an IR Spirit instrument (Shimadzu, Japan). Prior to conducting FT-IR, the lyophilized powder of AgNPs, PVA-NLCs, ENR@PVA-NLCs and ENR@PVA-NLCs/AgNPs were mixed with KBr at a ratio of 1:150 and pressed into a pellet using a high-pressure hydraulic machine. The infrared scanning wave numbers were from 4000 to 500 cm^{-1}.

2.4.5. X-ray diffraction

The crystalline structure of Ge, AgNPs, ENR, PVA-NLCs, ENR@PVA-NLCs and ENR@PVA-NLCs/AgNPs was determined with X-ray diffraction (XRD) patterns by a MiniFlex 600 instrument (Rigaku, Japan). Briefly, the aforementioned samples were placed in a crucible and compacted on a glass slide. Subsequently, XRD equipped with a Cu/Kα radiation source was performed at 4°/min in the scanning range of 5° ~ 50° under the conditions of 40 kV/40 mA.

2.4.6. UV–visible spectroscopy

Ultraviolet-visible spectrophotometry (UV-1900, Shimadzu, Japan) was used in the wavelength between 200 and 700 nm to analyze the UV spectral spectrum of the PVA-NLCs, ENR@PVA-NLCs, AgNPs and ENR@PVA-NLCs/AgNPs.

2.4.7. Rheological test

The viscosity of undiluted emulsions (PVA-NLCs, ENR@PVA-NLCs and ENR@PVA-NLCs/AgNPs) was measured using a rheometer (HAAKE MARS, Thermo Electron Corp., Germany). The measurements were carried out at 25 °C using the coaxial cylinder sensor (DG41). The flow behavior, shear stress and viscosity measures were determined by applying a continuous variation in the shear rate from 0.01 to 1000 s^{-1} (upward, downward and upward ramp). Newton's model (Eq. (1)) was adjusted to the rheological data.

$$\tau = \eta\,\gamma \tag{1}$$

where τ is the shear stress (mPa); η is the absolute viscosity (mPa·s); and γ is the shear rate (s^{-1}).

2.5. Encapsulation efficiency and drug loading of ENR@PVA-NLCs/AgNPs

The encapsulation efficiency and drug loading of ENR@PVA-NLCs/AgNPs was determined by the ultrafiltration centrifugation and UV spectrophotometry. Briefly, 0.5 mL of 1:10 diluent by 0.1 M NaOH (solubilize free/unencapsulated ENR) was put into the inner chamber of ultrafiltration centrifugal tube (MWCO: 100 kDa, Millipore, USA), followed by centrifugation at 5000 rpm for 20 min at 4 °C using a centrifuge (3 K15, Sigma, Germany). The filtrate in the outer chamber was diluted and determined as the amounts of free ENR. Moreover, ENR@PVA-NLCs/AgNPs diluent was ultrasonically demulsified and centrifuged for 10 min, then the supernatant was analyzed by UV spectrophotometry to obtain the total amount of ENR. The computational formula of the encapsulation efficiency (2) and drug loading (3) is as follows:

$$\text{Encapsulation efficiency} = (1 - \text{the amounts of free ENR/the total amount of ENR}) \times 100\% \tag{2}$$

$$\text{Drug loading} = (\text{the total amount of ENR/the total weight of emulsion}) \times 100\% \tag{3}$$

2.6. In vitro release of ENR and Ag^+ from ENR@PVA-NLCs/AgNPs

3 mL of ENR@PVA-NLCs/AgNPs were transferred into a dialysis bag (MWCO: 8000–14,000 Da, Yuanye Bio-Technology Co., Ltd., Shanghai, China) and kept in PBS (pH 7.2, 500 mL) on a shaking table at 37 °C for 24 h. After 5 mL of PBS was collected at different time points (0.5 h, 1 h,

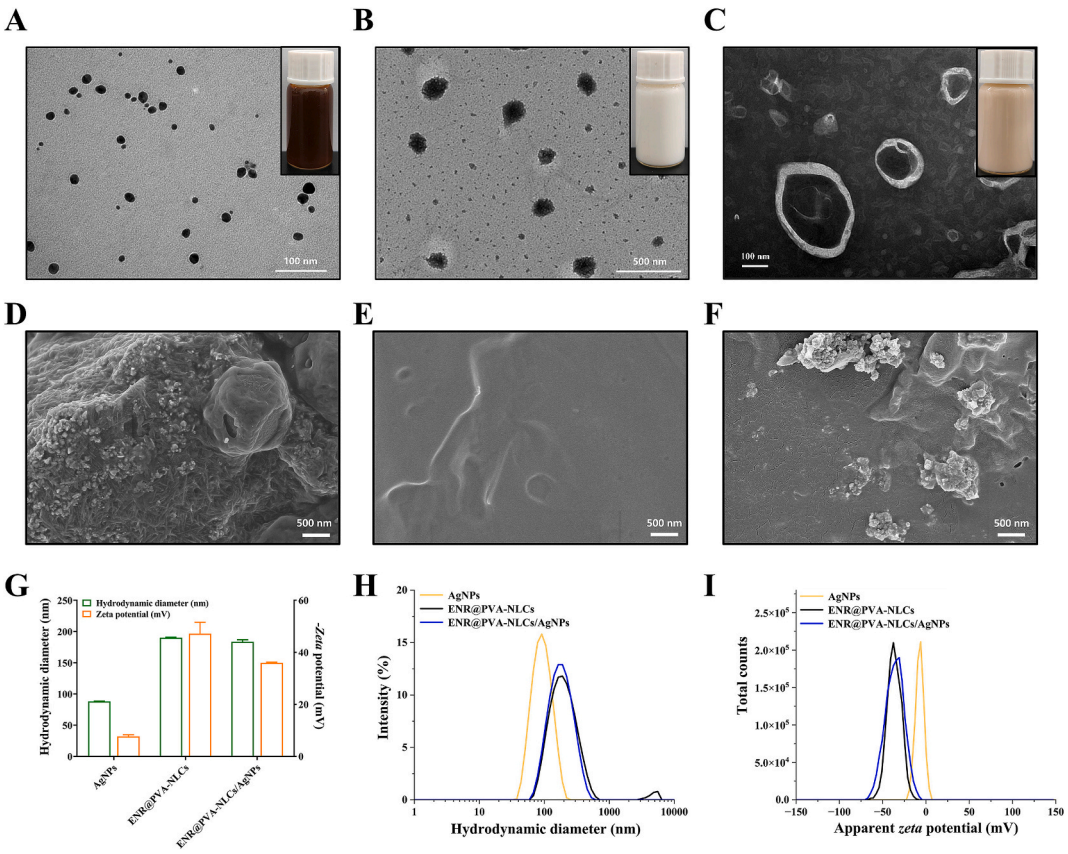

Fig. 1. Morphological and DLS characterization of ENR@PVA-NLCs/AgNPs. TEM images and appearance (insert) of AgNPs (A), ENR@PVA-NLCs (B) and ENR@PVA-NLCs/AgNPs (C). SEM images of AgNPs (D), ENR@PVA-NLCs (E) and ENR@PVA-NLCs/AgNPs (F). (G) Hydrodynamic diameter and *zeta* potential of ENR@PVA-NLCs/AgNPs. Particle size (H) and *zeta* potential (I) distribution of ENR@PVA-NLCs/AgNPs.

2 h, 4 h, 8 h, 12 h, 24 h), 5 mL of fresh PBS was added to keep the solution volume constant. The release efficiency of ENR was measured by UV–vis at 271 nm, and the content of Ag^+ was determined by atomic absorption spectroscopy (novAA350, Analytik Jena AG, Germany).

2.7. *In vitro antibacterial activity*

The antibacterial activity of ENR@PVA-NLCs/AgNPs was determined by the minimal inhibitory concentration (MIC) and minimal bactericidal concentration (MBC). Briefly, Ge, AgNPs, ENR, PVA-NLCs, ENR@PVA-NLCs, and ENR@PVA-NLCs/AgNPs were serially diluted with MH media and mixed with bacterial suspension (10^6 CFU/mL). The cultures were incubated for 24 h at 37 °C. The lowest dose without visible bacterial growth was defined as the MIC. Then the incubated cultures were swabbed on agar plates and incubated for 24 h. The lowest dose without bacterial growth was recorded as the MBC. Further, an Oxford cup assay was performed. Inoculums were adjusted to 10^6 CFU/mL, followed by uniform spreading on agar plates. 1 × MIC of AgNPs, ENR@PVA-NLCs, and ENR@PVA-NLCs/AgNPs were added to the cups. The inhibition zones were observed after 24 h of incubation. To investigate the growth kinetics of *E. coli*, *S. aureus* and *P. aeruginosa* in the presence of ENR@PVA-NLCs/AgNPs, 0.5 × MIC of the ENR@PVA-NLCs/AgNPs were added to the bacterial suspension (10^6 CFU/mL). Bacterial growth was monitored using absorbance (OD_{600}) measurements hourly with a microplate reader (Infinite M200 Pro, Tecan, Switzerland). In addition, to further explore the disruption effect of ENR@PVA-NLCs/AgNPs against bacterial cell walls, scanning electron microscopy (SEM; SU8010, Hitachi, Japan) were performed. Briefly, *E. coli* and *S. aureus* in the logarithmic phase was treated with a 2 × MIC dose of AgNPs, ENR@PVA-NLCs, and ENR@PVA-NLCs/AgNPs for 4 h, followed by centrifugation for 8 min at 5000 rpm. The supernatant was removed, and bacterial samples were washed, dehydrated, and dried for morphological observation.

2.8. *Checkerboard titration for synergy testing*

According to broth microdilution (Park et al., 2023), checkerboard titrations were performed to assess for synergy between ENR@PVA-NLCs and AgNPs against *E. coli*, *S. aureus* and *P. aeruginosa*. Concentrations of ENR@PVA-NLCs and AgNPs were varied using twofold serial dilutions according to their MIC against the respective bacteria. After the treatment, wells were observed visually and recorded for any visual growth. The clear wells as compared to growth controls were considered as combinations that against bacteria. Synergy was evaluated by calculating the fractional inhibitory concentration (FIC) index according to following formulas (4), (5) and (6):

$$\mathrm{FIC_{AgNPs}} = (\text{MIC of ENR@PVA} - \text{NLCs/AgNPs combination}) \div (\text{MIC of AgNPs alone}) \quad (4)$$

$$\mathrm{FIC_{ENR@PVA-NLCs}} = (\text{MIC of ENR@PVA} - \text{NLCs/AgNPs combination}) \div (\text{MIC of ENR@PVA} - \text{NLCs alone}) \quad (5)$$

$$\text{FIC index} = \mathrm{FIC_{AgNPs}} + \mathrm{FIC_{ENR@PVA-NLCs.}} \quad (6)$$

FIC index values ≤ 0.5 correspond to synergy, FIC index between 0.5 and 1 corresponds to additive, FIC index values between 1 and 4 correspond to indifference, and FIC index>4 corresponds to antagonism.

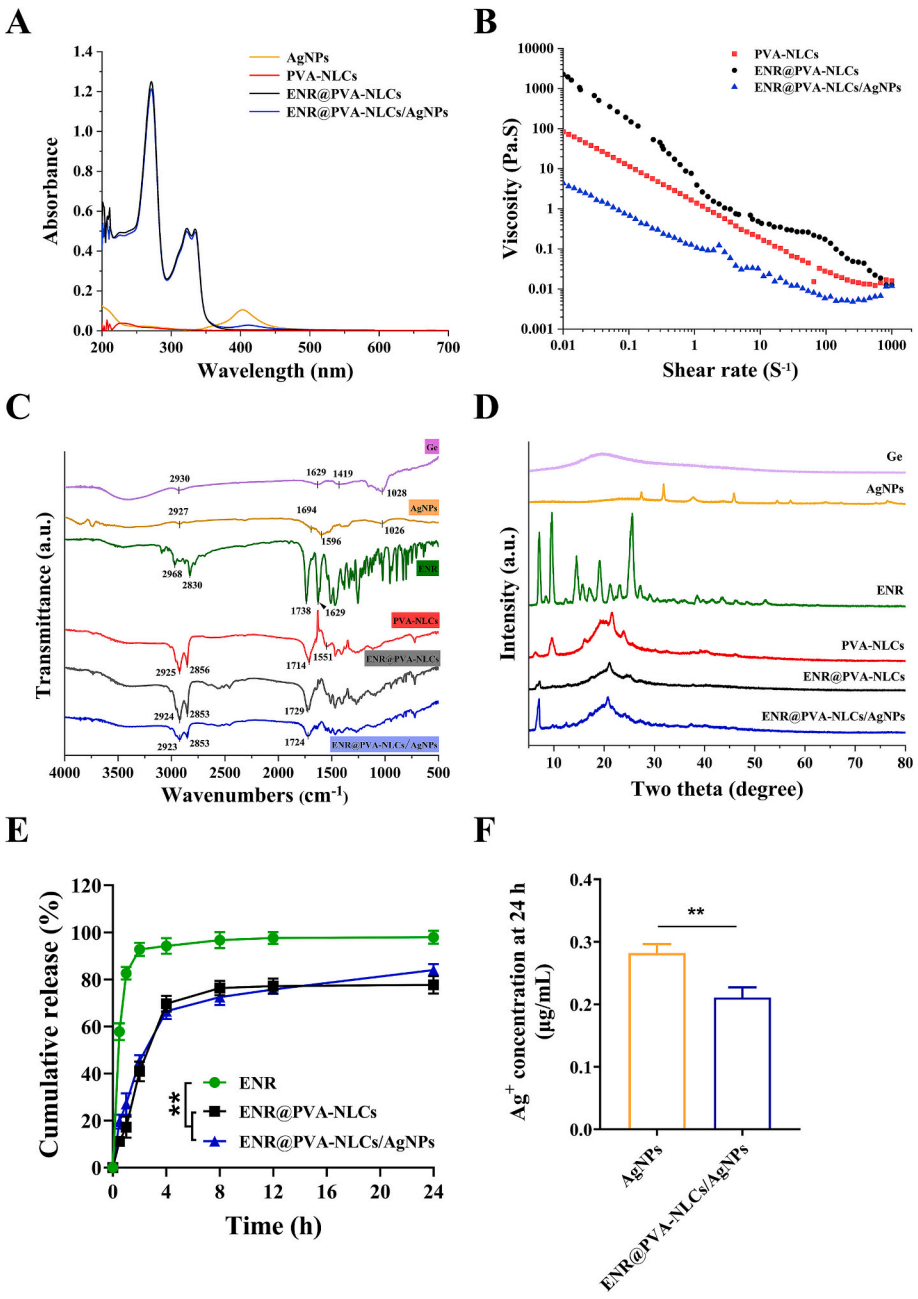

Fig. 2. Characterization of ENR@PVA-NLCs/AgNPs. (A) UV–vis spectrum of ENR@PVA-NLCs/AgNPs. (B) Shear viscosity of ENR@PVA-NLCs/AgNPs. (C) FTIR spectrum of ENR@PVA-NLCs/AgNPs. (D) XRD patterns of ENR@PVA-NLCs/AgNPs. (E) The release curves of ENR during a duration of 24 h, **indicates $P < 0.01$ *vs* ENR@PVA-NLCs/AgNPs and ENR@PVA-NLCs group. (F) The released content of Ag^{+} at 24 h.

2.9. Cell viability assay

CCK-8 test kit (Biosharp, Hefei, China) was utilized to examine the cell viability in the various treatment (PVA-NLCs, AgNPs, PVA-NLCs/AgNPs, ENR@PVA-NLCs, and ENR@PVA-NLCs/AgNPs). Firstly, BJ cells were adjusted to a density of 5000 cells per well and incubated for 24 h. Then the medium was changed to a different concentration of above-mentioned treatment. After culture for 24 h, 10 vol% CCK-8 were added to each well and incubated at 37 °C for 1.5 h, the absorbance at 450 nm (OD_{450}) was measured using a microplate reader (Infinite M200 Pro, Tecan, Switzerland). And the cell viability was calculated according to the following formula (7):

$$\text{Cell viability} = (OD_{treated} - OD_{blank})/(OD_{untreated} - OD_{blank}) \times 100\% \quad (7)$$

2.10. In vitro wound healing

The *in vitro* wound healing assay was performed referring to the previous study with some modification (Zuo et al., 2024). BJ cells (10^5 cells/well) were seeded into six-well plates and incubated for 24 h. Afterward, a straight-line scratch was made utilizing a 200-μL micropipette tip. Subsequently, debris was washed with PBS, and fresh DMEM containing 1 % FBS was added to the cells. As for experimental group, the medium contains PVA-NLCs, ENR@PVA-NLCs, AgNPs and ENR@PVA-NLCs/AgNPs, respectively. After 0 and 24 h, the scratch wound areas were photographed utilizing an inverted phase-contrast microscope (Leica DMi8, Wetzlar, Germany) and analyzed by ImageJ software. A_0 is the area of the initial scratch, and A_{24} is the area after treatment for 24 h. The migration rate was quantified by the formula (8):

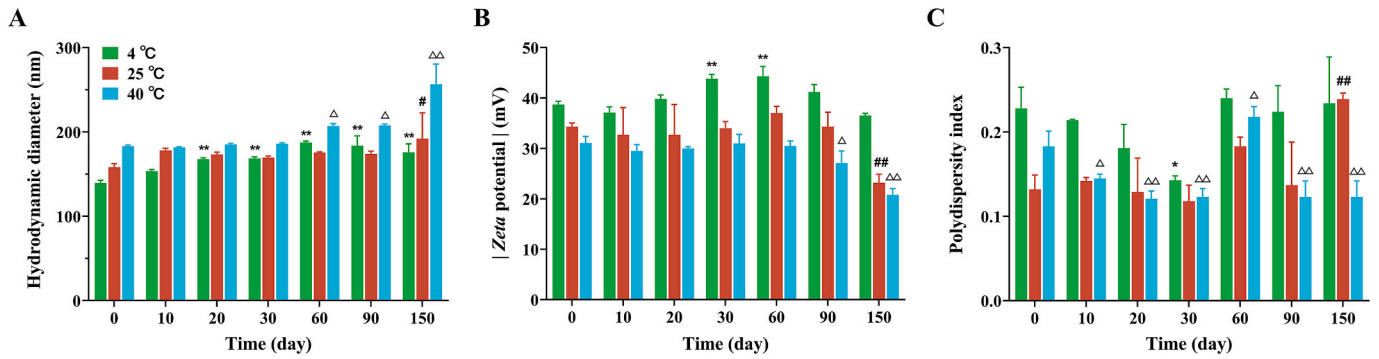

Fig. 3. The storage stability of ENR@PVA-NLCs/AgNPs. The hydrodynamic diameters (A), *zeta* potentials (B) and polydispersity indices (C) of ENR@PVA-NLCs/AgNPs at different temperatures and times. *indicates $P < 0.05$ *vs* Control (4 °C, 0 day) group, **indicates $P < 0.01$. #indicates $P < 0.05$ *vs* Control (25 °C, 0 day) group, ##indicates $P < 0.01$. △indicates $P < 0.05$ *vs* Control (40 °C, 0 day) group, △△indicates $P < 0.05$.

$$\text{Migration rate}\ (\%) = (A_0 - A_{24})/A_0 \times 100\% \quad (8)$$

2.11. *In vivo wound healing evaluation*

All animal experiments were approved by the Institutional Animal Care and Use Committee of Nanjing Agricultural University and comply with all ethical regulations. The Sprague-Dawley male rats (200 ± 20 g) were acclimatized into the experimental setting for a week. A circular skin wound of 2.0 cm in diameter was established on the back of rat using a scalpel after it was anesthetized by the inhalation of isoflurane. Then 200 μL of *S. aureus* suspension (10^8 CFU/mL) was added to the wound surface. Three days later, the rats were randomly divided into five groups (n = 6), 40 μL of PBS, PVA-NLCs, AgNPs, ENR@PVA-NLCs, and ENR@PVA-NLCs/AgNPs was applied evenly to the infected wound before covering it with a disposable retention film and then medical gauze dressing to secure it. The wounds were photographed for up to 9 days. To evaluate the *in vivo* antibacterial activity of ENR@PVA-NLCs/AgNPs, 50 mg of wound tissues were collected, crushed, and spread on the Tryptone Soy Agar (TSA) plates. Moreover, the wound tissues were excised and processed into Hematoxylin-eosin (HE) and Masson-stained sections for histological evaluation. To study the expression level of Collagen III, transforming growth factor-β (TGF-β), and vascular endothelial growth factor (VEGF) in infected wound sites, immunohistochemical staining method was applied and the obtained results were quantified using Image J software.

2.12. *Statistical analysis*

The experimental data are expressed as Mean ± SD. Statistical comparisons were performed by SPSS 19.0 software. One way ANOVA followed by Tukey's multiple comparison tests (post-hoc tests) was used for all experimental calculation. Differences with one same letter of the label are not significant ($P > 0.05$), and differences with different letters of the label are significant ($P < 0.05$).

3. Results and discussion

3.1. *Characterization of ENR@PVA-NLCs/AgNPs*

The resulting AgNPs exhibited a spherical morphology with the size of 17.40 ± 7.66 nm (Fig. 1A), and the appearance of AgNPs solution was reddish-brown, which is different from the light-yellow Ge solution (Gong et al., 2023). In addition, ENR@PVA-NLCs/AgNPs and ENR@PVA-NLCs had a near spherical structure with similar size, consistent with dynamic light scattering (DLS) results (Fig. 1B–C&G–H). However, the appearance of ENR@PVA-NLCs/AgNPs was different from that of ENR@PVA-NLCs. And the former is light-brown, the latter is white. Scanning electron microscopy (SEM) images revealed that the ENR@PVA-NLCs exhibited a smooth surface structure and was similar to previous reports (Saghafi et al., 2021; Song et al., 2016; Trucillo et al., 2022). The morphology of AgNPs was spherical aggregation and displayed a rough surface structure. Importantly, we found that the aggregations of AgNPs was on the surface of ENR@PVA-NLCs, preliminarily confirming the successful fabrication of ENR@PVA-NLCs/AgNPs (Fig. 1D–F). In terms of *zeta* potential, AgNPs, ENR@PVA-NLCs, and ENR@PVA-NLCs/AgNPs exhibited different *zeta* potentials of −7.68 ± 0.62 mV, −37.14 ± 0.46 mV, and − 36.00 ± 0.20 mV respectively (Fig. 1G&I).

To further validate the successful synthesis of ENR@PVA-NLCs/AgNPs, ultraviolet spectral analysis was conducted. The results demonstrate that PVA-NLCs did not exhibit apparent absorption peak, and ENR@PVA-NLCs and ENR@PVA-NLCs/AgNPs both exhibit absorption peaks at 271 and 314 nm, which aligns with the characteristic absorption peaks of ENR as reported in literature (Lizondo et al., 1997). It is noteworthy that the distinctive peak of AgNPs emerges at 402 nm, and the weak peak of ENR@PVA-NLCs/AgNPs emerges at 411 nm (Fig. 2A), which both attribute to the presence of nano-silver (Prathna et al., 2011) and indicate that the majority of AgNPs were incorporated in ENR@PVA-NLCs. Notably particularly, a temperature sensitivity was observed in ENR@PVA-NLCs/AgNPs at a phase transition temperature with 4 °C (solid state) and 30 °C (liquid state) (Fig. S1). According to Fig. 2B, the apparent viscosities of nano-emulsions decreased with the increase of shear rate, showing the phenomenon of shear thinning, which belonged to a pseudoplastic fluid (non-Newtonian fluid). Significantly, the viscosity of PVA-NLCs increased after the addition of ENR, which is due to an enhancement in the forces that interact with the constituents. And ENR@PVA-NLCs/AgNPs had a lowest viscosity, ensuring ease of application and spreadability on the skin (Mahadev et al., 2025). The FT-IR spectra of ENR@PVA-NLCs/AgNPs and its individual components was showed in Fig. 2C. In the spectrum of AgNPs, the characteristic peaks at 1629 and 1419 cm^{-1} for Ge disappeared, and new peak at 1596 cm^{-1} were displayed, which may be attributed to the interaction between AgNPs with C═O functional groups (1629 cm^{-1}) of Ge. Besides, ENR showed broad O—H stretching bands at 2968, 2830 cm^{-1} which indicates the presence of carboxylic acid (Kumar et al., 2014). And the characteristic peak at 1629 $cm^{-1}$was attributed to C═O stretching absorption (Kumar et al., 2014). Through the comparison with the FTIR spectra of ENR, ENR@PVA-NLCs and ENR@PVA-NLCs/AgNPs, the FTIR spectrum of ENR@PVA-NLCs and ENR@PVA-NLCs/AgNPs showed the adsorption peak at 1729–1724 cm^{-1}, which moved to higher frequencies with reduced intensities and the disappeared peaks at 1629 cm^{-1}, indicated that ENR are encapsulated in NLCs and the successful preparation of ENR@PVA-NLCs and ENR@PVA-NLCs/AgNPs. In Fig. 2D, the pattern of Ge exhibited amorphous nature without characteristic peak, whereas AgNPs were shown to be in crystalline form, and Bragg reflections were observed. Four distinct

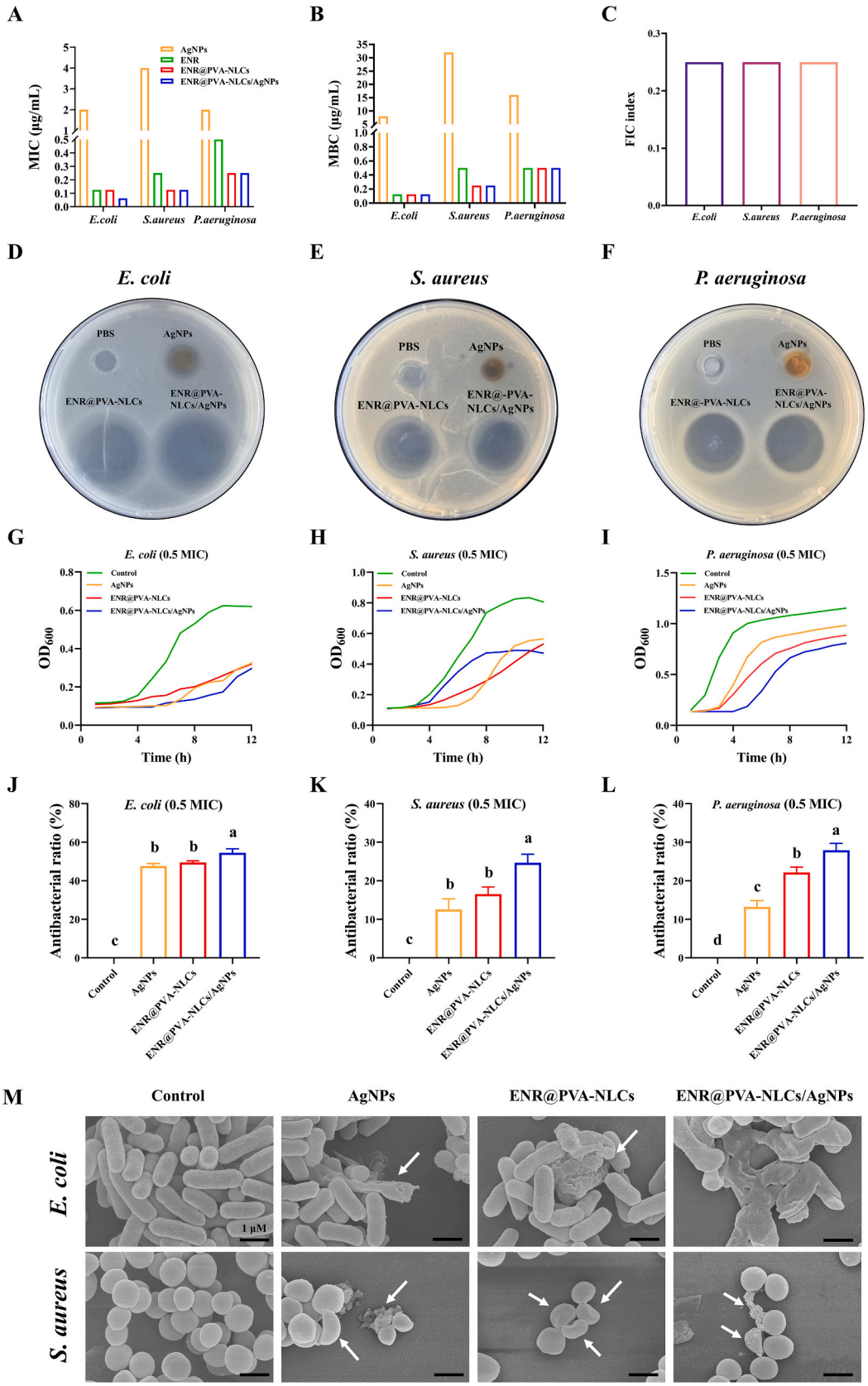

Fig. 4. *In vitro* antibacterial activity of ENR@PVA-NLCs/AgNPs. The MIC (A) and MBC (B) of ENR@PVA-NLCs/AgNPs against *E. coli*, *S. aureus* and *P. aeruginosa*. (C) FIC indices to assess synergy between AgNPs and ENR@PVA-NLCs. (D–F) Oxford cup assay. (G–I) Growth monitoring curves. (J–L) Antibacterial ratio of 0.5 MIC of ENR@PVA-NLCs/AgNPs. Differences with one same letter of the label are not significant ($P > 0.05$), and differences with different letters of the label are significant ($P < 0.05$). (M) SEM images of bacterial morphological upon ENR@PVA-NLCs/AgNPs treatment.

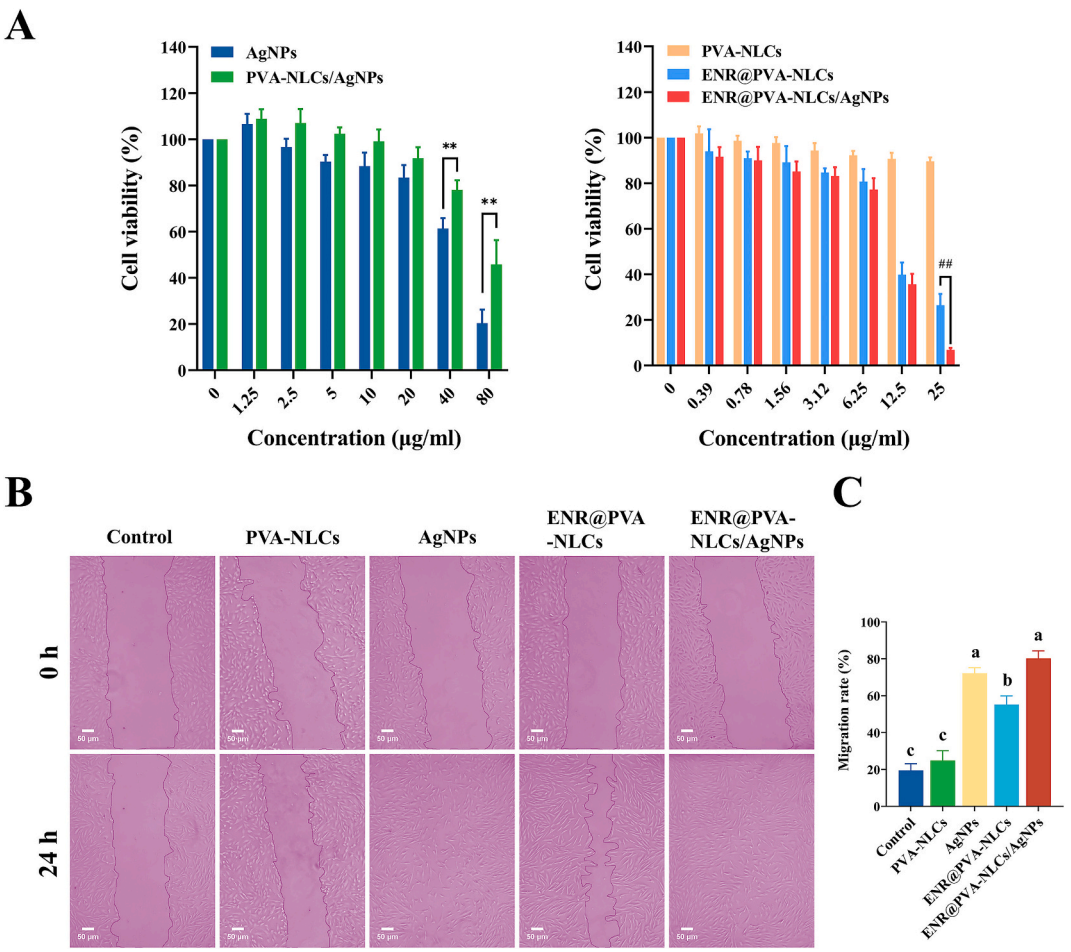

Fig. 5. *In vitro* wound healing activity of ENR@PVA-NLCs/AgNPs. (A) Cytotoxicity of AgNPs, PVA-NLCs/AgNPs, ENR@PVA-NLCs, and ENR@PVA-NLCs/AgNPs in BJ cells. **indicates $P < 0.01$ between AgNPs *vs* PVA-NLCs/AgNPs group. And ##indicates $P < 0.01$ between ENR@PVA-NLCs and ENR@PVA-NLCs/AgNPs group. (B) Microscopic images of cell migration captured after 24 h of treatment with ENR@PVA-NLCs/AgNPs. (C) The effect of ENR@PVA-NLCs/AgNPs on migration of BJ cells. Differences with one same letter of the label are not significant ($P > 0.05$), and differences with different letters of the label are significant ($P < 0.05$).

diffraction peaks located at 37.83°, 45.82°, 64.18° and 76.40° were assigned to the (111), (200), (220) and (311) planes, respectively, corresponded to the planes of the face-centered cubic (FCC) crystal lattice of metallic silver (JCPDS No. 04-0783) (Siddique et al., 2024). Moreover, the pattern of ENR displayed diffraction peaks at 7.11°, 9.60° and 14.52°, indicating that ENR was a crystalline structure. In the pattern of ENR@PVA-NLCs and ENR@PVA-NLCs/AgNPs, the above characteristic diffraction peaks of ENR were weakened or disappearing, indicating a structure change of the ENR in the NLCs. And the diffraction peaks of AgNPs also disappeared in ENR@PVA-NLCs/AgNPs. Furthermore, the diffraction pattern of the PVA-NLCs matched the ENR@PVA-NLCs and ENR@PVA-NLCs/AgNPs, showing that the ENR and AgNPs were encapsulated in the NLCs. Encapsulation efficiency (EE) and drug loading (DL) are important indexes to evaluate the quality of drug carriers (Wang et al., 2017). In this study, the standard curve of ENR was firstly established by ultraviolet-visible spectroscopy (UV–Vis) method (Fig. S2), then calculated EE and DL of ENR@PVA-NLCs/AgNPs were 80.66 ± 4.59 % and 1.21 ± 0.07 %, respectively. Notably, the amount of ENR in ENR@PVA-NLCs/AgNPs was 12.40 ± 0.68 mg/mL, which is much higher than the solubility of ENR in pure water (<0.5 mg/mL) (Lizondo et al., 1997), indicating that PVA-NLCs could improve the solubility of ENR. As shown in Fig. 2E, the cumulative release rate of the ENR@PVA-NLCs and ENR@PVA-NLCs/AgNPs from 0 to 24 h was similar and lower than that of ENR, demonstrating the slow-release characteristic of the ENR@PVA-NLCs and ENR@PVA-NLCs/AgNPs. In terms of the release of Ag^+, the released silver content of ENR@PVA-NLCs/AgNPs in PBS for 24 h was 0.282 ± 0.014 μg/mL and less than that of AgNPs (Fig. 2F), indicating that embedding AgNPs into NLCs endow them with controlled release of silver ions and thus reduced potential toxicity.

The stability of nanomedicine is a critical factor for effective biological application (Shakeel and Ramadan, 2010). In this study, the storage stability of ENR@PVA-NLCs/AgNPs were evaluated, based on desired characteristics such as hydrodynamic diameter (HD), polydispersity index (PDI) and *zeta* potential. We found that ENR@PVA-NLCs/AgNPs had the optimal storage stability at 25 °C during the storage period of 90 days (Fig. 3).

3.2. *In vitro* antibacterial activity of ENR@PVA-NLCs/AgNPs

Ge and PVA-NLCs had no antibacterial activity within the set concentration range (not shown), while the MICs of AgNPs against above bacteria was 2–4 μg/mL, and the MBCs ranged from 8 to 32 μg/mL (Fig. 4A–B). Besides, ENR had more potent antibacterial activity than AgNPs, and the MICs of ENR ranged from 0.125 to 0.5 μg/mL, which was similar to the MBCs. It is noteworthy that the MICs of ENR@PVA-NLCs and ENR@PVA-NLCs/AgNPs was neck and neck (Fig. 4A), and they are almost both lower than that of ENR, indicating the more potent antibacterial activity. Considering *in vitro* drug release property, the encapsulation of ENR by NLCs could achieve doses decreasing and antibacterial efficacy increasing. To investigate the antimicrobial synergy between ENR@PVA-NLCs and AgNPs in ENR@PVA-NLCs/AgNPs,

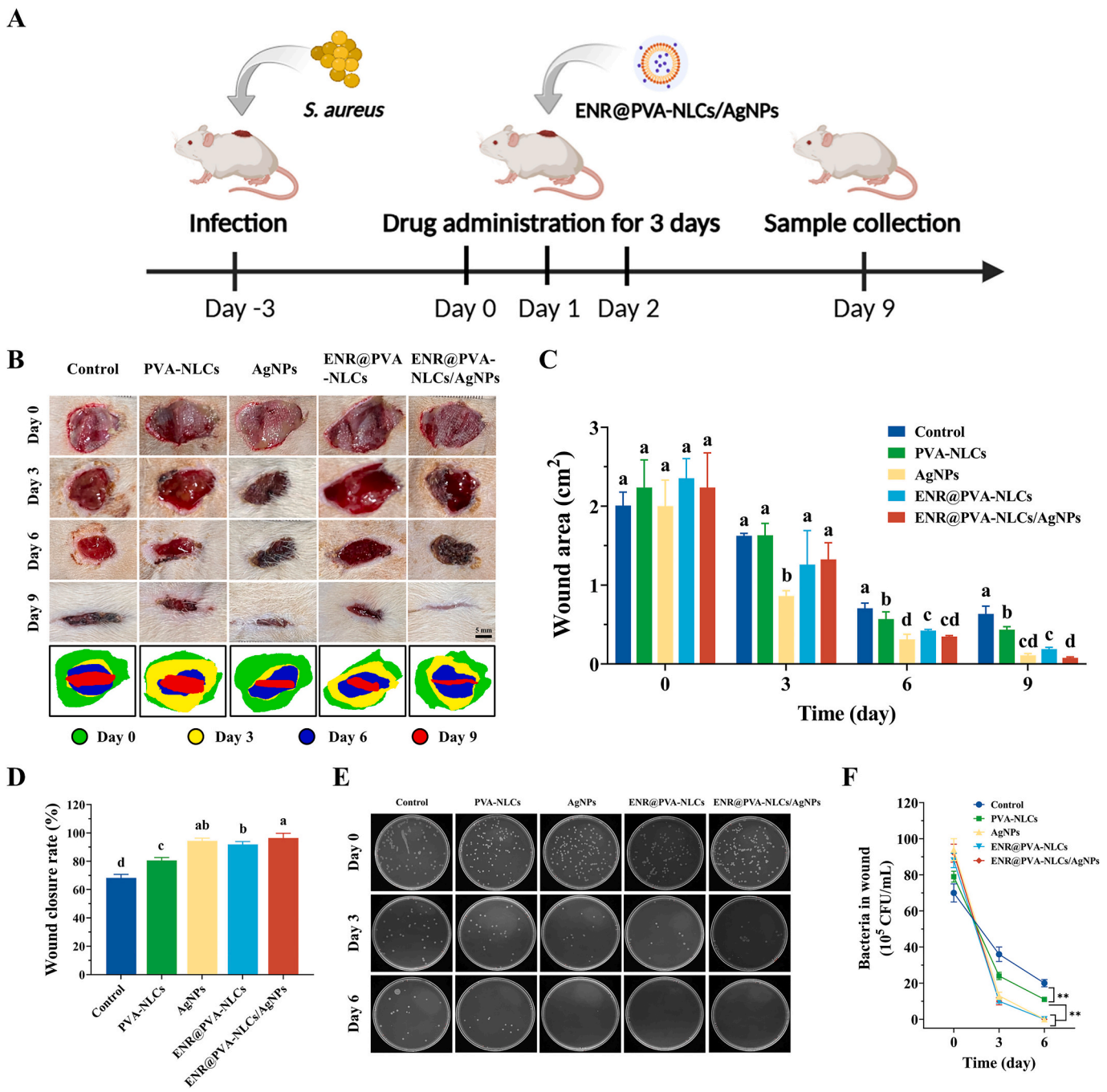

Fig. 6. *In vivo* wound healing efficacy of ENR@PVA-NLCs/AgNPs. (A) Schematic illustration of the establishment of wound infection model and the overall experimental process. (B) The photographs and of *S. aureus*-infected skin wound treated with ENR@PVA-NLCs/AgNPs. (C) The change of skin wound area. (D) Closure rate of infected wounds on day 9. (E) Representative colony formation plates. Differences with one same letter of the label are not significant ($P > 0.05$), and differences with different letters of the label are significant ($P < 0.05$). (F) The quantitative results of plate colony forming unit counts. **indicates $P < 0.01$.

the fractional inhibitory concentration (FIC) index was quantified. In Fig. 4C and Tables S1–S3, synergy between ENR@PVA-NLCs and AgNPs was observed. The synergistic activity of the ENR@PVA-NLCs/AgNPs demonstrates the promise of combination therapy through lipid nanoparticle-assisted delivery of ENR and AgNPs. To further verify the antibacterial efficacy of ENR@PVA-NLCs/AgNPs, Oxford cup assay was performed. An obvious inhibition zone was noted with AgNPs, ENR@PVA-NLCs and ENR@PVA-NLCs/AgNPs, demonstrating their powerful antibacterial potential (Fig. 4D–F). Notably, ENR@PVA-NLCs and ENR@PVA-NLCs/AgNPs had stronger antibacterial efficacy. To further quantify the synergistic antibacterial activity, the bacterial growth curves were performed, we found that 0.5 MIC of ENR@PVA-NLCs/AgNPs had more potent inhibitory effect, compared to treatments with 0.5 MIC of AgNPs or ENR@PVA-NLCs (Fig. 4G–L). This progression in antibacterial activity highlights the enhanced bioavailability and efficacy of ENR@PVA-NLCs and underscores the potent synergism achieved by incorporating AgNPs. Last, scanning electron microscopy (SEM) was employed to observe the morphology of bacteria treated with various nanoparticles. The results revealed that *E. coli* and *S. aureus* in the control group maintained their original rod-shaped and round-shaped structures with smooth surfaces; however, upon treatment with AgNPs, ENR@PVA-NLCs, and ENR@PVA-NLCs/AgNPs, all

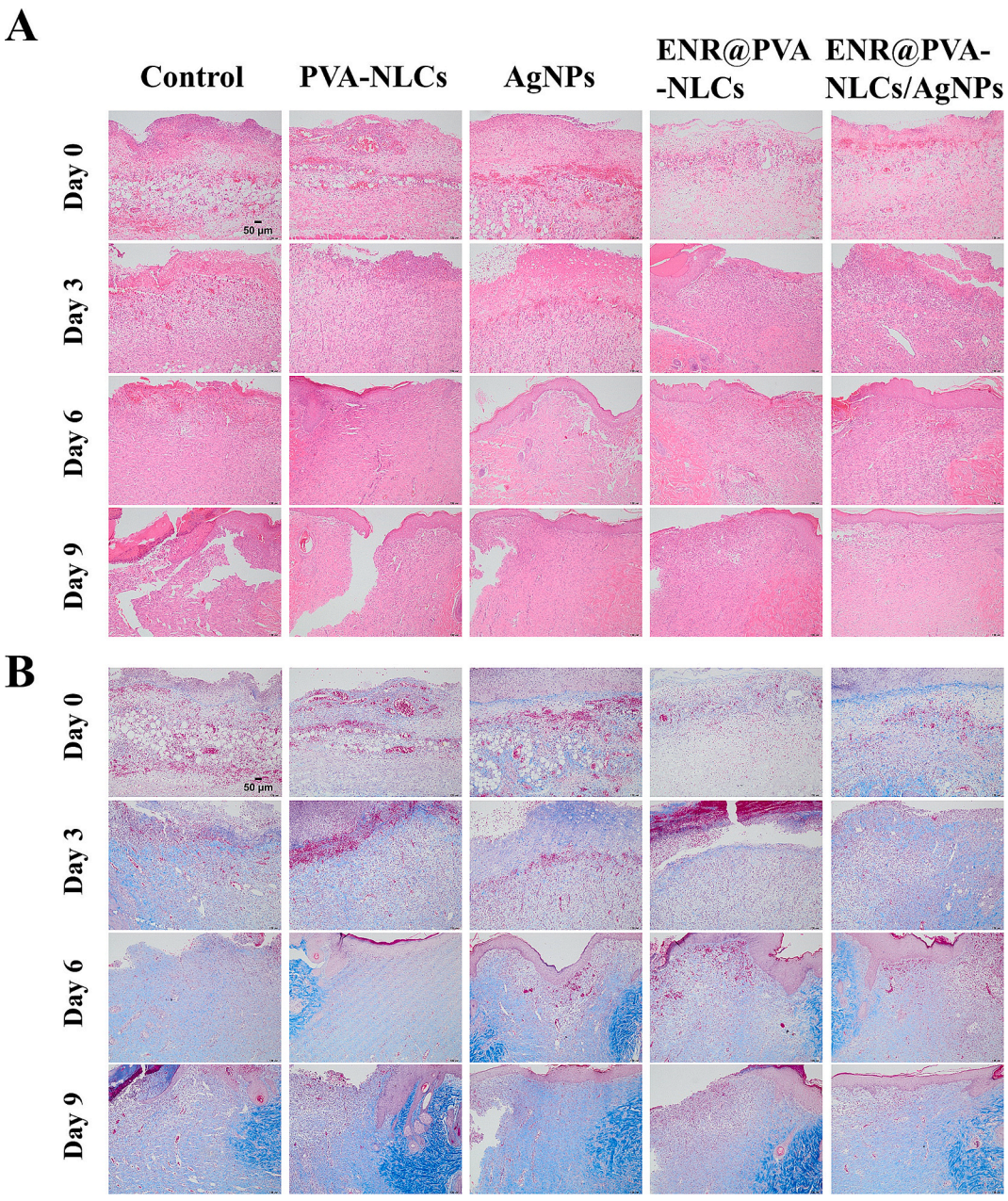

Fig. 7. The HE staining (A) and Masson's trichrome staining (B) of skin wounds after different treatments on day 0, 3, 6 and 9.

groups exhibited significant changes in bacterial morphology - particularly evident in *E. coli* and *S. aureus* from the group treated with ENR@PVA-NLCs/AgNPs which displayed severe rupture (Fig. 4M). The SEM images of bacteria directly demonstrated the remarkable synergistic antibacterial efficacy of ENR@PVA-NLCs/AgNPs, exhibiting superior bactericidal potency compared to AgNPs and ENR@PVA-NLCs. The enhanced antimicrobial efficacy can be attributed to chelation-mediated interactions between hydroxyl groups in ENR and AgNPs, forming a stable ENR-AgNPs conjugate. This hybrid nanostructure consists of a metallic silver core encapsulated by enrofloxacin molecules through coordination bonding, which facilitates targeted accumulation of antimicrobial agents at the infection site and amplifies bactericidal potency (Li et al., 2005). In addition, in view of the fact that microorganisms have been reported to develop resistance to ENR with AgNPs (Gunawan et al., 2017; Panácek et al., 2018; Sobkowich et al., 2025; Teichmann et al., 2025), future studies are needed to investigate whether ENR@PVA-NLCs/AgNPs induce bacterial resistance.

3.3. *In vitro* wound healing study

To assess the clinical application potential, cytotoxicity of ENR@PVA-NLCs/AgNPs was evaluated by CCK-8 assay against BJ cells *in vitro*. As shown in Fig. 5A, the viability of BJ cells incubated with AgNPs, PVA-NLCs/AgNPs, ENR@PVA-NLCs and ENR@PVA-NLCs/AgNPs decreased in a dose-dependent manner, while those cells incubated with PVA-NLCs exhibited no cytotoxicity even when exposed to concentrations up to 25 μg/mL. It is worth noting that PVA-NLCs/AgNPs have better biocompatibility than AgNPs at 40 and 80 μg/mL, which indicate PVA-NLCs lowered the toxicity of AgNPs and is also the key benefit of PVA-NLCs, compared with many similar reports (Feng et al., 2019; Shao et al., 2015; Torres-Mendieta et al., 2022; Wijesundera et al., 2022; Xiong et al., 2022). We attributed this phenomenon to the slow-release behavior of Ag ions (Fig. 2F). Panášek et al. also reported similar results in their investigations where silver covalently bound to cyanographene (GCN/Ag) showed an enhanced cell viability as

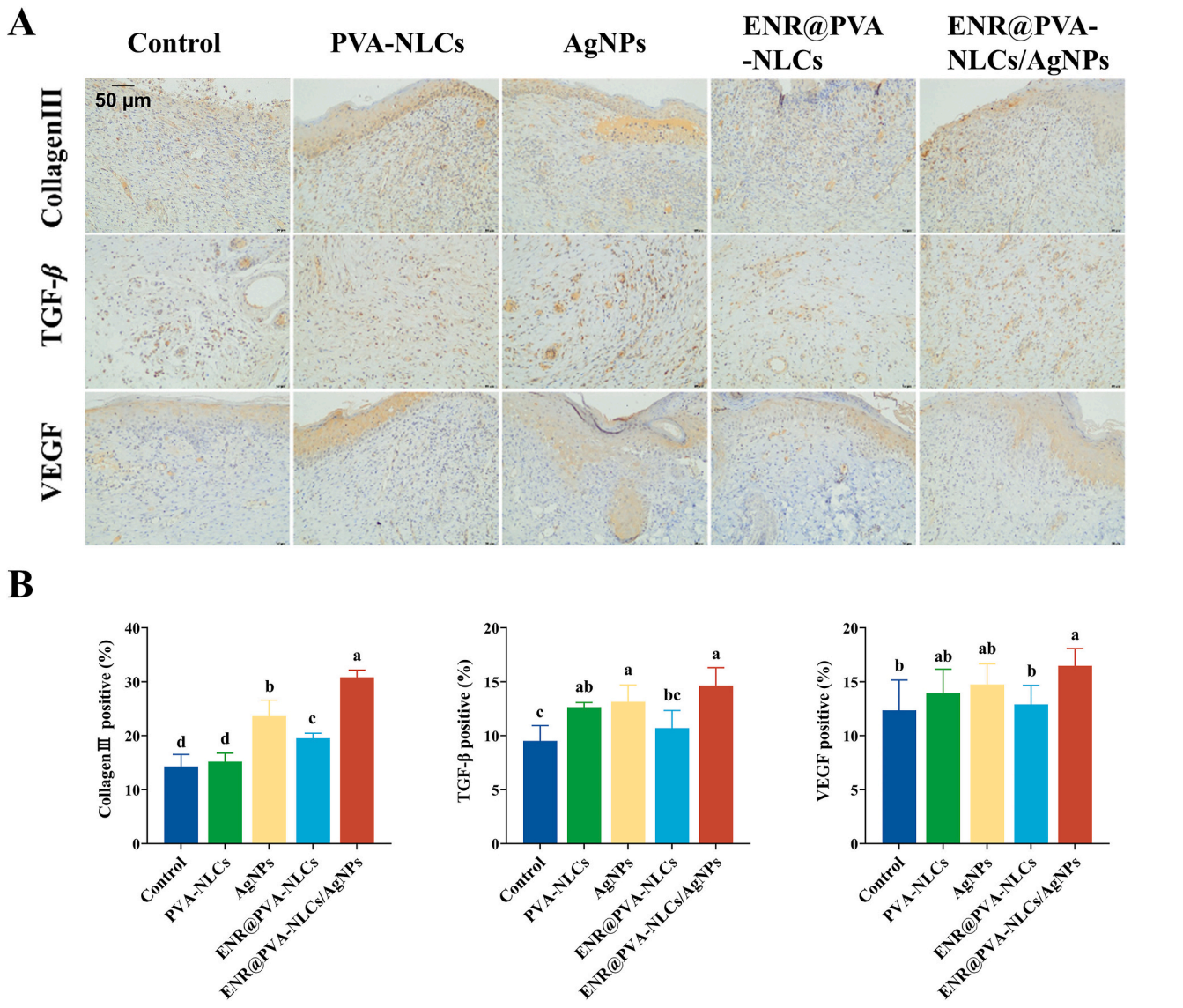

Fig. 8. IHC analysis of the wound tissues on day 9 post injury. (A) VEGF, TGF-β and Collagen III staining of skin tissue sections. (B) Expression levels of VEGF, TGF-β and Collagen III quantified by ImageJ. Differences with one same letter of the label are not significant ($P > 0.05$), and differences with different letters of the label are significant ($P < 0.05$).

compared to AgNPs colloids (Panacek et al., 2021). In addition, we observed that upon increasing the ENR concentration of ENR@PVA-NLCs and ENR@PVA-NLCs/AgNPs from 1.56 to 25 μg/mL, the cell viability was reduced to <90 %. And the ENR@PVA-NLCs and ENR@PVA-NLCs/AgNPs at 0.78 μg/mL do not affect cell viability, indicating their good biocompatibility at their MIC.

One of the crucial criteria of an ideal wound dressing is enhancement of epidermal migration (Mohanty et al., 2023). The effect on migration of BJ cells on exposure to ENR@PVA-NLCs/AgNPs was determined using wound scratch test *in vitro* (Fig. 5B–C). ENR@PVA-NLCs/AgNPs exhibited a higher rate of cell migration compared to ENR@PVA-NLCs. This increased rate of cell migration could be majorly attributed to the presence of AgNPs. The results obtained can be explained by a study conducted by Chinnasamy et al., which reported that biosynthetic silver nanoparticles had potential wound healing activity (Chinnasamy et al., 2019). Therefore, it can be concluded from migration assays that prepared ENR@PVA-NLCs/AgNPs perhaps help in remodeling of cells if used as a wounds dressing.

3.4. *In vivo wound healing study*

The antibacterial activity of ENR@PVA-NLCs/AgNPs *in vivo* and their effects on promoting wound healing was evaluated. Fig. 6A presents a schematic diagram of the process of wound infection with *S. aureus* ATCC 29213, the ENR@PVA-NLCs/AgNPs treatment, and then healing. As depicted in Fig. 6B–C, the wound area gradually decreased in rat that received the AgNPs, ENR@PVA-NLCs and ENR@PVA-NLCs/AgNPs, comparing to control-treated rat. Moreover, interestingly, the wound area of NLCs-treated rat also decreased on day 6, speculating that NLCs can form a single-layer membrane on the skin surface, which can keep the skin moist, reduce skin moisture loss, and thus be more conducive to wound healing (Motsoene et al., 2023). In Fig. 6D, the wound closure rate was (68.36 ± 2.43) % by day 9 in control group, and (96.49 ± 3.27) % in the ENR@PVA-NLCs/AgNPs treatment group, higher than that of ENR@PVA-NLCs (92.00 ± 2.00) % and AgNPs (94.51 ± 1.79) %. And there was no significant difference between AgNPs and ENR@PVA-NLCs/AgNPs groups in wound healing ability, indicating that the addition of AgNPs into ENR@PVA-NLCs maintain the wound healing potential of AgNPs. Of note, the bacterial counts at the

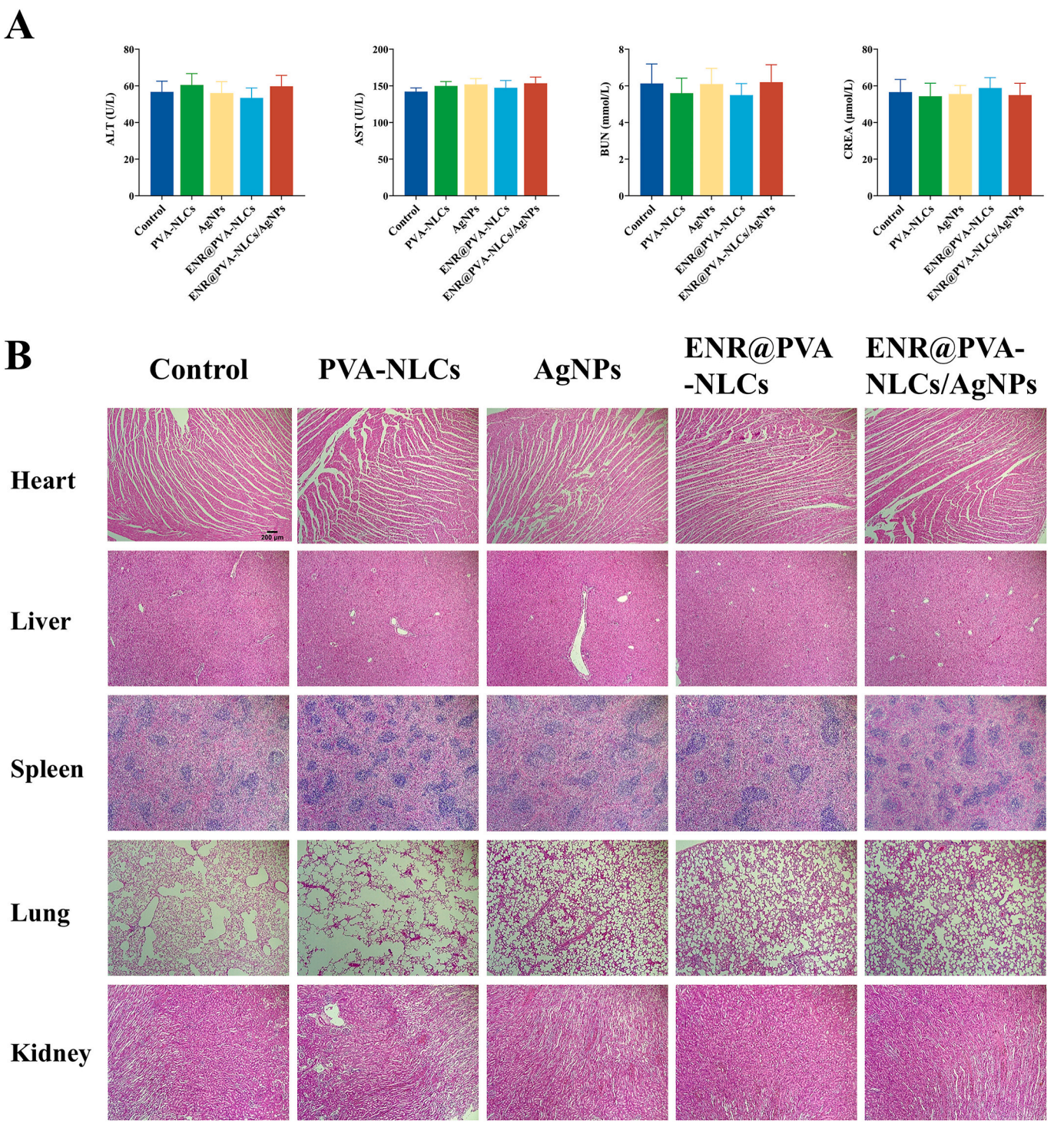

Fig. 9. *In vivo* biosafety of ENR@PVA-NLCs/AgNPs. (A) Blood biochemistry results (ALT, AST, BUN and CREA) and (B) HE staining images of the heart, liver, spleen, lung and kidney of rat treated with ENR@PVA-NLCs/AgNPs.

wound site on day 6 in the Control group and NLCs treatment group were significantly higher than that in the AgNPs, ENR@PVA-NLCs and ENR@PVA-NLCs/AgNPs treatment group (Fig. 6E–F). From the above results, we found that ENR@PVA-NLCs/AgNPs still played a strong synergistically antibacterial effect in rats, and the presence of AgNPs endow ENR@PVA-NLCs enhanced wound healing efficacy.

To further investigate the mechanism of wound healing, the histological examination was evaluated. The skin layer morphology and collagen deposition were assessed by HE and Masson staining, respectively. As shown in Fig. 7A, H&E staining showed the skin tissue structure disordered, the epidermis was discontinuous, and many inflammatory cells infiltrated before treatment. On day 3, after treatment with AgNPs, ENR@PVA-NLCs and ENR@PVA-NLCs/AgNPs, inflammatory cell infiltration condition was significantly improved. On days 6 and 9, we found clearly confirmed full squamous epithelium, well-distributed neovascularization and new collagen fiber formation in the AgNPs and ENR@PVA-NLCs/AgNPs group, indicating an outstanding tissue-repair capacity of AgNPs and ENR@PVA-NLCs/AgNPs. Further, Masson staining assay was applied to evaluate the growth of collagen fibers. On day 9, an epidermal layer similar to the normal skin structure

was formed among AgNPs, ENR@PVA-NLCs and ENR@PVA-NLCs/AgNPs groups (Fig. 7B). Comparing the blue collagen fiber areas, it was found that the AgNPs group had the highest proportion, followed by the ENR@PVA-NLCs group and ENR@PVA-NLCs/AgNPs group. In a word, the above results indicate that the presence of AgNPs and ENR@PVA-NLCs in ENR@PVA-NLCs/AgNPs could accelerate the deposition of collagen fibers to promote wound healing.

Finally, immunohistochemistry was conducted to examine the expression of Collagen III, TGF-β and VEGF protein after different treatment. In Fig. 8A–B, the ENR@PVA-NLCs/AgNPs group exhibited the highest level of Collagen III, indicating that ENR@PVA-NLCs/AgNPs could promote the production of collagen. The TGF-β signaling pathway is regarded as a pivotal mechanism in tissue repair due to its close association with myofibrogenesis (Urban and Davis, 2014). The ENR@PVA-NLCs/AgNPs group exhibited a higher level of TGF-β than that of ENR@PVA-NLCs group, indicating the addition of AgNPs in ENR@PVA-NLCs might enhance collagen fiber production by upregulating TGF-β protein expression. The vascular endothelial growth factor (VEGF) plays a key role in neovascularization by stimulating endothelial cell proliferation, as well as enhancing vascular permeability (Apte et al., 2019). The ENR@PVA-NLCs/AgNPs group showed significantly elevated levels of VEGF expression compared to ENR@PVA-NLCs groups, suggesting that ENR@PVA-NLCs/AgNPs enhanced angiogenesis, thereby facilitating nutrient delivery to metabolically active wounds site. This elucidates the wound healing mechanism of ENR@PVA-NLCs/AgNPs, highlighting their potential as a therapeutic agent for treating wound infection.

3.5. Biocompatibility evaluation of ENR@PVA-NLCs/AgNPs

In addition to ensuring the effectiveness of the nano-formulations, one of the most important challenges to be addressed is biocompatibility (Singh et al., 2019). Previous reports have demonstrated that the interaction between AgNPs and cells could have adverse effects and cause cellular damage, *e.g. via* oxidative stress (Mat'atková et al., 2022). The oxidative stress resulting from nanoparticles' presence can contribute to inflammation, toxicity, and DNA damage and thus to the development of serious conditions like pulmonary inflammation or organs like kidney and liver issues (Dikshit et al., 2021). In this study, blood biochemistry assay and HE staining were used to evaluate the *in vivo* biosafety of ENR@PVA-NLCs/AgNPs. We found that all groups were within normal ranges and showed no significant changes, indicating that the ENR@PVA-NLCs/AgNPs did not have any substantial systemic toxicity that would affect liver and kidney functions (Fig. 9A). The administered PVA-NLCs, AgNPs, ENR@PVA-NLCs, and ENR@PVA-NLCs/AgNPs for rats showed no significant pathological changes in heart, liver, spleen, lung and kidney tissues when compared to the control group (Fig. 9B). Above promising findings suggest the great potential of ENR@PVA-NLCs/AgNPs as biocompatible dressings for infected wounds.

4. Conclusion

Herein, we utilized high pressure homogenization technique and successfully developed a scalable antibacterial nanoplatform, the poly (vinyl alcohol) modified enrofloxacin-silver composite nano-emulsion (ENR@PVA-NLCs/AgNPs). The optimal ENR@PVA-NLCs/AgNPs was shown to be thermosensitive, with slow release of ENR and Ag^{+}, and excellent biocompatibility. Moreover, ENR@PVA-NLCs/AgNPs effectively impeded the proliferation of *E. coli*, *S. aureus* and *P. aeruginosa in vitro*. The wound infection model in rats revealed that ENR@PVA-NLCs/AgNPs facilitated wound healing by accelerating collagen fiber deposition, enhancing angiogenesis and encouraging tissue remodeling. Taken together, our results confirmed that the antibacterial nanoplatform may be a potential candidate for wound infection dressing.

CRediT authorship contribution statement

Jiahao Gong: Writing – original draft, Methodology, Investigation, Conceptualization. **Moxin Liu:** Writing – original draft, Methodology, Investigation, Formal analysis. **Runan Zuo:** Writing – review & editing, Validation, Supervision, Resources. **Xinhao Song:** Resources, Methodology. **Junqi Wang:** Resources, Formal analysis. **Qindan Zuo:** Writing – review & editing, Resources. **Yan Jiang:** Software, Investigation. **Yunfeng Long:** Writing – review & editing, Supervision. **Yuzhen Silang:** Visualization, Validation. **Zeng Luo:** Validation, Resources. **Xiuge Gao:** Validation, Resources. **Dawei Guo:** Writing – review & editing, Supervision, Project administration, Funding acquisition.

Declaration of competing interest

The authors declare the following financial interests/personal relationships which may be considered as potential competing interests: Dawei Guo reports financial support was provided by National Natural Science Foundation of China.

Acknowledgements

This research was supported by Key Research and Development Program of Jiangsu Province (BE2022394), Collaborative Innovation Special Project of Regional Science and Technology in Tibet (QYXTZX-RKZ2024-03-2), the Fundamental Research Funds for the Central Universities (KYCXJC2024002), National Natural Science Foundation of China (31502120), and a Project Funded by the Priority Academic Program Development of Jiangsu Higher Education Institutions (PAPD).

Appendix A. Supplementary data

Supplementary data to this article can be found online at https://doi.org/10.1016/j.ijpx.2025.100330.

Data availability

Data will be made available on request.

References

Apte, R.S., Chen, D.S., Ferrara, N., 2019. VEGF in signaling and disease: beyond discovery and development. Cell 176 (6), 1248–1264. https://doi.org/10.1016/j.cell.2019.01.021.

Bochicchio, S., Lamberti, G., Barba, A.A., 2021. Polymer-lipid pharmaceutical nanocarriers: innovations by new formulations and production technologies. Pharmaceutics 13 (2). https://doi.org/10.3390/pharmaceutics13020198.

Chinnasamy, G., Chandrasekharan, S., Bhatnagar, S., 2019. Biosynthesis of silver nanoparticles from melia azedarach: enhancement of antibacterial, wound healing, antidiabetic and antioxidant activities. Int. J. Nanomedicine 14, 9823–9836. https://doi.org/10.2147/IJN.S231340.

Dikshit, P.K., Kumar, J., Das, A.K., Sadhu, S., Sharma, S., Singh, S., Gupta, P.K., Kim, B.S., 2021. Green synthesis of metallic nanoparticles: applications and limitations. Catalysts 11 (8). https://doi.org/10.3390/catal11080902.

Du, X.J., Wang, J.L., Iqbal, S., Li, H.J., Cao, Z.T., Wang, Y.C., Du, J.Z., Wang, J., 2018. The effect of surface charge on oral absorption of polymeric nanoparticles. Biomater. Sci. 6 (3), 642–650. https://doi.org/10.1039/c7bm01096f.

Dubourg, G., Abat, C., Raoult, D., 2017. Why new antibiotics are not obviously useful now. Int. J. Antimicrob. Agents 49 (5), 549–553. https://doi.org/10.1016/j.ijantimicag.2016.11.015.

Feng, Y., Wang, G., Chang, Y., Cheng, Y., Sun, B., Wang, L., Chen, C., Zhang, H., 2019. Electron compensation effect suppressed silver ion release and contributed safety of Au@Ag core-shell nanoparticles. Nano Lett. 19 (7), 4478–4489. https://doi.org/10.1021/acs.nanolett.9b01293.

Gainza, G., Pastor, M., Aguirre, J.J., Villullas, S., Pedraz, J.L., Hernandez, R.M., Igartua, M., 2014. A novel strategy for the treatment of chronic wounds based on the topical administration of rhEGF-loaded lipid nanoparticles: in vitro bioactivity and in vivo effectiveness in healing-impaired db/db mice. J. Control. Release 185, 51–61. https://doi.org/10.1016/j.jconrel.2014.04.032.

Gao, X.G., Gong, J.H., Cai, Y., Wang, J.C., Wen, J., Peng, L., Ji, H., Jiang, S.X., Guo, D.W., 2021. Chitosan modified squalene nanostructured lipid carriers as a promising adjuvant for freeze-dried ovalbumin vaccine. Int. J. Biol. Macromol. 188, 855–862. https://doi.org/10.1016/j.ijbiomac.2021.08.074.

Gokce, E.H., Korkmaz, E., Dellera, E., Sandri, G., Bonferoni, M.C., Ozer, O., 2012. Resveratrol-loaded solid lipid nanoparticles versus nanostructured lipid carriers: evaluation of antioxidant potential for dermal applications. Int. J. Nanomedicine 7, 1841–1850. https://doi.org/10.2147/IJN.S29710.

Gong, J., Cheng, X., Zuo, J., Zhang, Y., Lin, J., Liu, M., Jiang, Y., Long, Y., Si, H., Gao, X., Guo, D., Gu, N., 2023. Silver nanoparticles combat Salmonella Typhimurium: Suppressing intracellular infection and activating dendritic cells. Colloids Surf. B: Biointerfaces 226, 113307. https://doi.org/10.1016/j.colsurfb.2023.113307.

Gunawan, C., Marquis, C.P., Amal, R., Sotiriou, G.A., Rice, S.A., Harry, E.J., 2017. Widespread and indiscriminate nanosilver use: genuine potential for microbial resistance. ACS Nano 11 (4), 3438–3445. https://doi.org/10.1021/acsnano.7b01166.

He, X., Chen, F., Chang, Z., Waqar, K., Hu, H., Zheng, X., Wang, Y., Dong, W.F., Yang, C., 2022. Silver mesoporous silica nanoparticles: fabrication to combination therapies for cancer and infection. Chem. Rec. 22 (4), e202100287. https://doi.org/10.1002/tcr.202100287.

Ibraheem, D.R., Hussein, N.N., Sulaiman, G.M., Mohammed, H.A., Khan, R.A., Al Rugaie, O., 2022. Ciprofloxacin-loaded silver nanoparticles as potent nano-antibiotics against resistant pathogenic bacteria. Nanomaterials 12 (16). https://doi.org/10.3390/nano12162808.

Ibraheem, D.R., Alwas, N.G.A., Dawood, R.A., Nasser, S.M., Abbood, S.H., Sulaiman, G. M., Jabir, M.S., Mohammed, H.A., Ghotekar, S., 2024. Inhibitory effect of silver nanoparticles–conjugated PEG-nystatin against some resistance pathogenic bacteria. Inorg. Chem. Commun. 168. https://doi.org/10.1016/j.inoche.2024.112952.

Jawad, K.H., Jamagh, F.K., Sulaiman, G.M., Hasoon, B.A., Albukhaty, S., Mohammed, H. A., Abomughaid, M.M., 2024. Antibacterial and antibiofilm activities of amikacin-conjugated gold nanoparticles: a promising formulation for contact lens preservation. Inorg. Chem. Commun. 162. https://doi.org/10.1016/j.inoche.2024.112286.

Jiji, S., Udhayakumar, S., Maharajan, K., Rose, C., Muralidharan, C., Kadirvelu, K., 2020. Bacterial cellulose matrix with in situ impregnation of silver nanoparticles via catecholic redox chemistry for third degree burn wound healing. Carbohydr. Polym. 245, 116573. https://doi.org/10.1016/j.carbpol.2020.116573.

Khairnar, S.V., Pagare, P., Thakre, A., Nambiar, A.R., Junnuthula, V., Abraham, M.C., Kolimi, P., Nyavanandi, D., Dyawanapelly, S., 2022. Review on the scale-up methods for the preparation of solid lipid nanoparticles. Pharmaceutics 14 (9). https://doi.org/10.3390/pharmaceutics14091886.

Khutoryanskiy, V.V., 2018. Beyond PEGylation: alternative surface-modification of nanoparticles with mucus-inert biomaterials. Adv. Drug Deliv. Rev. 124, 140–149. https://doi.org/10.1016/j.addr.2017.07.015.

Kumar, G.P., Phani, A.R., Prasad, R.G., Sanganal, J.S., Manali, N., Gupta, R., Rashmi, N., Prabhakara, G.S., Salins, C.P., Sandeep, K., Raju, D.B., 2014. Polyvinylpyrrolidone oral films of enrofloxacin: film characterization and drug release. Int. J. Pharm. 471 (1–2), 146–152. https://doi.org/10.1016/j.ijpharm.2014.05.033.

Lee, S.H., Jun, B.H., 2019. Silver nanoparticles: synthesis and application for nanomedicine. Int. J. Mol. Sci. 20 (4). https://doi.org/10.3390/ijms20040865.

Li, P., Li, J., Wu, C.Z., Wu, Q.S., Li, J., 2005. Synergistic antibacterial effects of β-lactam antibiotic combined with silver nanoparticles. Nanotechnology 16 (9), 1912–1917. https://doi.org/10.1088/0957-4484/16/9/082.

Li, X., Montague, E.C., Pollinzi, A., Lofts, A., Hoare, T., 2022. Design of smart size-, surface-, and shape-switching nanoparticles to improve therapeutic efficacy. Small 18 (6), e2104632. https://doi.org/10.1002/smll.202104632.

Liang, Z., Chen, D., 2022. Targeting therapy effects of composite hyaluronic acid/chitosan nanosystems containing inclusion complexes. Drug Deliv. 29 (1), 2734–2741. https://doi.org/10.1080/10717544.2022.2112995.

Liu, X.L., Lee, P.Y., Ho, C.M., Lui, V.C.H., Chen, Y., Che, C.M., Tam, P.K.H., Wong, K.K.Y., 2010. Silver nanoparticles mediate differential responses in keratinocytes and fibroblasts during skin wound healing. Chemmedchem 5 (3), 468–475. https://doi.org/10.1002/cmdc.200900502.

Liu, Y., Chen, D., Zhang, A., Xiao, M., Li, Z., Luo, W., Pan, Y., Qu, W., Xie, S., 2021. Composite inclusion complexes containing hyaluronic acid/chitosan nanosystems for dual responsive enrofloxacin release. Carbohydr. Polym. 252, 117162. https://doi.org/10.1016/j.carbpol.2020.117162.

Lizondo, M., Pons, M., Gallardo, M., Estelrich, J., 1997. Physicochemical properties of enrofloxacin. J. Pharm. Biomed. Anal. 15 (12), 1845–1849. https://doi.org/10.1016/s0731-7085(96)02033-x.

Luo, W., Jiang, Y., Liu, J., Ju, M., Algharib, S.A., Dawood, A.S., 2023. On-demand release of enrofloxacin-loaded chitosan oligosaccharide-oxidized hyaluronic acid composite nanogels for infected wound healing. Int. J. Biol. Macromol. 253 (Pt 6), 127248. https://doi.org/10.1016/j.ijbiomac.2023.127248.

Mahadev, M., Ballal, S., Shetty, A., Dubey, A., Shetty, S.S., Hebbar, S., El-Zahaby, S.A., 2025. Development and evaluation of chitosan-coated virgin coconut oil-asiatic acid-loaded nanoemulgel for enhanced wound management. Int. J. Biol. Macromol. 299. https://doi.org/10.1016/j.ijbiomac.2025.140097.

Mat'atková, O., Michailidu, J., Miskovská, A., Kolouchová, I., Masák, J., Cejková, A., 2022. Antimicrobial properties and applications of metal nanoparticles biosynthesized by green methods. Biotechnol. Adv. 58. https://doi.org/10.1016/j.biotechadv.2022.107905.

Meng, K., Chen, D., Yang, F., Zhang, A., Tao, Y., Qu, W., Pan, Y., Hao, H., Xie, S., 2020. Intracellular delivery, accumulation, and discrepancy in antibacterial activity of four enrofloxacin-loaded fatty acid solid lipid nanoparticles. Colloids Surf. B: Biointerfaces 194, 111196. https://doi.org/10.1016/j.colsurfb.2020.111196.

Mohanty, S., Bharadwaj, T., Verma, D., Paul, S., 2023. Development of Ag doped ZnO nanostructure and tranexamic acid infused chitosan-guargum film: a multifunctional antimicrobial dressing with haemostatic and wound closure potential. Chem. Eng. J. 472. https://doi.org/10.1016/j.cej.2023.144976.

Motsoene, F., Abrahamse, H., Dhilip Kumar, S.S., 2023. Multifunctional lipid-based nanoparticles for wound healing and antibacterial applications: a review. Adv. Colloid Interf. Sci. 321, 103002. https://doi.org/10.1016/j.cis.2023.103002.

Pallavicini, P., Arciola, C.R., Bertoglio, F., Curtosi, S., Dacarro, G., D'Agostino, A., Ferrari, F., Merli, D., Milanese, C., Rossi, S., Taglietti, A., Tenci, M., Visai, L., 2017. Silver nanoparticles synthesized and coated with pectin: an ideal compromise for anti-bacterial and anti-biofilm action combined with wound-healing properties. J. Colloid Interface Sci. 498, 271–281. https://doi.org/10.1016/j.jcis.2017.03.062.

Panácek, A., Kvítek, L., Smékalová, M., Vecerová, R., Kolár, M., Röderová, M., Dycka, F., Sebela, M., Prucek, R., Tomanec, O., Zboril, R., 2018. Bacterial resistance to silver nanoparticles and how to overcome it. Nat. Nanotechnol. 13 (1), 65–+. https://doi.org/10.1038/s41565-017-0013-y.

Panacek, D., Hochvaldová, L., Bakandritsos, A., Malina, T., Langer, M., Belza, J., Martincová, J., Vecerová, R., Lazar, P., Pólaková, K., Kolarík, J., Válková, L., Kolár, M., Otyepka, M., Panacek, A., Zboril, R., 2021. Silver covalently bound to cyanographene overcomes bacterial resistance to silver nanoparticles and antibiotics. Adv. Sci. 8 (12). https://doi.org/10.1002/advs.202003090.

Pang, Y.P., Zhao, M.F., Xie, Y.H., Wang, Y.P., You, Y.X., Ke, Y.D., Zhang, C.Y., Chen, X. H., Yang, Y.J., Zhang, C.L., Chen, X., Liu, Y., Fang, X.T., 2024. Multifunctional Ac@ZIF-8/AgNPs nanoplatform with pH-responsive and ROS scavenging antibacterial properties promotes infected wound healing. Chem. Eng. J. 489. https://doi.org/10.1016/j.cej.2024.151485.

Park, J., Nabawy, A., Doungchawee, J., Mahida, N., Foster, K., Jantarat, T., Jiang, M., Chattopadhyay, A.N., Hassan, M.A., Agrohia, D.K., Makabenta, J.M., Vachet, R.W., Rotello, V.M., 2023. Synergistic treatment of multidrug-resistant bacterial biofilms using silver nanoclusters incorporated into biodegradable nanoemulsions. ACS Appl. Mater. Interfaces 15 (31), 37205–37213. https://doi.org/10.1021/acsami.3c06242.

Paudel, S., Peña-Bahamonde, J., Shakiba, S., Astete, C.E., Louie, S.M., Sabliov, C.M., Rodrigues, D.F., 2021. Prevention of infection caused by enteropathogenic *E. coli* O157:H7 in intestinal cells using enrofloxacin entrapped in polymer based nanocarriers. J. Hazard. Mater. 414. https://doi.org/10.1016/j.jhazmat.2021.125454.

Prathna, T.C., Chandrasekaran, N., Raichur, A.M., Mukherjee, A., 2011. Biomimetic synthesis of silver nanoparticles by Citrus limon (lemon) aqueous extract and theoretical prediction of particle size. Colloids Surf. B: Biointerfaces 82 (1), 152–159. https://doi.org/10.1016/j.colsurfb.2010.08.036.

Rai, M., Yadav, A., Gade, A., 2009. Silver nanoparticles as a new generation of antimicrobials. Biotechnol. Adv. 27 (1), 76–83. https://doi.org/10.1016/j.biotechadv.2008.09.002.

Rolim, W.R., Pieretti, J.C., Renó, D.L.S., Lima, B.A., Nascimento, M.H.M., Ambrosio, F. N., Lombello, C.B., Brocchi, M., de Souza, A.C.S., Seabra, A.B., 2019. Antimicrobial activity and cytotoxicity to tumor cells of nitric oxide donor and silver nanoparticles containing PVA/PEG films for topical applications. ACS Appl. Mater. Interfaces 11 (6), 6589–6604. https://doi.org/10.1021/acsami.8b19021.

Ruennarong, N., Wongpanit, K., Sakulthaew, C., Giorgi, M., Kumagai, S., Poapolathep, A., Poapolathep, S., 2016. Dispositions of enrofloxacin and its major metabolite ciprofloxacin in Thai swamp buffaloes. J. Vet. Med. Sci. 78 (3), 397–403. https://doi.org/10.1292/jvms.15-0464.

Saghafi, Z., Mohammadi, M., Mahboobian, M.M., Derakhshandeh, K., 2021. Preparation, characterization, and in vivo evaluation of perphenazine-loaded nanostructured lipid carriers for oral bioavailability improvement. Drug Dev. Ind. Pharm. 47 (3), 509–520. https://doi.org/10.1080/03639045.2021.1892745.

Shakeel, F., Ramadan, W., 2010. Transdermal delivery of anticancer drug caffeine from water-in-oil nanoemulsions. Colloids Surf. B: Biointerfaces 75 (1), 356–362. https://doi.org/10.1016/j.colsurfb.2009.09.010.

Shao, W., Liu, X.F., Min, H.H., Dong, G.H., Feng, Q.Y., Zuo, S.L., 2015. Preparation, characterization, and antibacterial activity of silver nanoparticle-decorated graphene oxide nanocomposite. ACS Appl. Mater. Interfaces 7 (12), 6966–6973. https://doi.org/10.1021/acsami.5b00937.

Siddique, A.B., Amr, D., Abbas, A., Zohra, L., Irfan, M.I., Alhoshani, A., Ashraf, S., Amin, H.M.A., 2024. Synthesis of hydroxyethylcellulose phthalate-modified silver nanoparticles and their multifunctional applications as an efficient antibacterial, photocatalytic and mercury-selective sensing agent. Int. J. Biol. Macromol. 256 (Pt 1), 128009. https://doi.org/10.1016/j.ijbiomac.2023.128009.

Singh, A.P., Biswas, A., Shukla, A., Maiti, P., 2019. Targeted therapy in chronic diseases using nanomaterial-based drug delivery vehicles. Signal Transduct. Target. Ther. 4, 33. https://doi.org/10.1038/s41392-019-0068-3.

Sobkowich, K.E., Hui, A.Y., Poljak, Z., Szlosek, D., Plum, A., Weese, J.S., 2025. Nationwide analysis of methicillin-resistant staphylococci in cats and dogs: resistance patterns and geographic distribution. Am. J. Vet. Res. 86 (3). https://doi.org/10.2460/ajvr.24.09.0253.

Song, J., Fan, X.C., Shen, Q., 2016. Daidzein-loaded nanostructured lipid carriers-PLGA nanofibers for transdermal delivery. Int. J. Pharm. 501 (1–2), 245–252. https://doi.org/10.1016/j.ijpharm.2016.02.003.

Suo, H.N., Hussain, M., Wang, H., Zhou, N.Y., Tao, J., Jiang, H., Zhu, J.T., 2021. Injectable and pH-sensitive hyaluronic acid-based hydrogels with on-demand release of antimicrobial peptides for infected wound healing (vol 22, pg 3049, 2021). Biomacromolecules 22 (12), 5400. https://doi.org/10.1021/acs.biomac.1c01487.

Tao, Y., Yang, F., Meng, K., Chen, D., Yang, Y., Zhou, K., Luo, W., Qu, W., Pan, Y., Yuan, Z., Xie, S., 2019. Exploitation of enrofloxacin-loaded docosanoic acid solid lipid nanoparticle suspension as oral and intramuscular sustained release formulations for pig. Drug Deliv. 26 (1), 273–280. https://doi.org/10.1080/10717544.2019.1580798.

Teichmann, L., Pasman, R., Luitwieler, S., Varriale, C., Bengtsson-Palme, J., Ter Kuile, B., 2025. Adaptation of Escherichia coli to ciprofloxacin and enrofloxacin: Differential proteomics of the SOS response and RecA-independent mechanisms. Int. J.

Antimicrob. Agents 65 (2), 107420. https://doi.org/10.1016/j.ijantimicag.2024.107420.
Torres-Mendieta, R., Nguyen, N.H.A., Guadagnini, A., Semerad, J., Lukowiec, D., Parma, P., Yang, J., Agnoli, S., Sevcu, A., Cajthaml, T., Cernik, M., Amendola, V., 2022. Growth suppression of bacteria by biofilm deterioration using silver nanoparticles with magnetic doping. Nanoscale 14 (48), 18143–18156. https://doi.org/10.1039/d2nr03902h.
Trucillo, P., Sofia, D., Cortese, L., Urciuolo, M., 2022. Production of Q10+B2 nanostructured lipid carriers and optimization of their entrapment capacities. Colloids Surf. B Biointerfaces 217. https://doi.org/10.1016/j.colsurfb.2022.112653.
Urban, Z., Davis, E.C., 2014. Cutis laxa: intersection of elastic fiber biogenesis, TGFbeta signaling, the secretory pathway and metabolism. Matrix Biol. 33, 16–22. https://doi.org/10.1016/j.matbio.2013.07.006.
Wang, T., Xue, J., Hu, Q., Zhou, M., Luo, Y., 2017. Preparation of lipid nanoparticles with high loading capacity and exceptional gastrointestinal stability for potential oral delivery applications. J. Colloid Interface Sci. 507, 119–130. https://doi.org/10.1016/j.jcis.2017.07.090.
Wijesundera, S.A., Jayawardana, K.W., Yan, M., 2022. Trehalose-modified silver nanoparticles as antibacterial agents with reduced cytotoxicity and enhanced uptake by mycobacteria. ACS Appl. Nano Mater. 5 (8), 10704–10714. https://doi.org/10.1021/acsanm.2c02047.
Xiong, J., Cao, Y., Zhao, H., Chen, J., Cai, X., Li, X., Liu, Y., Xiao, H., Ge, J., 2022. Cooperative antibacterial enzyme-Ag-polymer nanocomposites. ACS Nano 16 (11), 19013–19024. https://doi.org/10.1021/acsnano.2c07930.
Xu, X., Gao, S., Zuo, Q., Gong, J., Song, X., Liu, Y., Xiao, J., Zhai, X., Sun, H., Zhang, M., Gao, X., Guo, D., 2024. Enhanced in vitro antiviral activity of ivermectin-loaded nanostructured lipid carriers against porcine epidemic diarrhea virus via improved intracellular delivery. Pharmaceutics 16 (5). https://doi.org/10.3390/pharmaceutics16050601.
Yang, Z.F., Huang, R.K., Zheng, B.N., Guo, W.T., Li, C.K., He, W.Y., Wei, Y.G., Du, Y., Wang, H.M., Wu, D.C., Wang, H., 2021. Highly stretchable, adhesive, biocompatible, and antibacterial hydrogel dressings for wound healing. Adv. Sci. 8 (8). https://doi.org/10.1002/advs.202003627.
Zheng, B.D., Ye, J., Yang, Y.C., Huang, Y.Y., Xiao, M.T., 2022. Self-healing polysaccharide-based injectable hydrogels with antibacterial activity for wound healing. Carbohydr. Polym. 275, 118770. https://doi.org/10.1016/j.carbpol.2021.118770.
Zuo, R.N., Gong, J.H., Gao, X.G., Huang, J.H., Zhang, J.R., Jiang, S.X., Guo, D.W., 2024. Using halofuginone-silver thermosensitive nanohydrogels with antibacterial and anti-inflammatory properties for healing wounds infected with Staphylococcus aureus. Life Sci. 339, 122414. https://doi.org/10.1016/j.lfs.2024.122414.